IOSR Journal of Mechanical and Civil Engineering (IOSR-JMCE)
e-ISSN: 2278-1684,p-ISSN: 2320-334X, Volume 17, Issue 3 Ser. IV (May - June 2020), PP 26-47
www.iosrjournals.org

Evaluating and improving the blast resistance capacity of the RC fences

Mohamed A. Basset[1], Mohamed Abdelwahab[2], Khaled M. Abdelgawad[3], M. N. Fayed[4]
[1, 2, 4]*(Faculty of Engineering, Ain-Shams University, Egypt)*
[3]*(Lecturer of Civil Defense, Police Academy, Egypt)*

Abstract:
Background*: The purpose of using RC fences is to make a suitable distance between the explosion and the building, in order to reduce the damage that can occur in the building as much as possible, this distance is called stand-off distance. There are two common types of movable RC fences in Egypt, RC Curved and T-Shaped fences, which can be used to provide the protection for important buildings against blast loads.*
Materials and Methods*: In this paper, Numerical analyses for blasting different RC fences were performed using LS-DYNA program. Basic considerations are presented for five constitutive material models (the concrete material, the reinforcing steel material, the air material, the rigid material, the CFRP and the high-energy explosive material) also the Equations of state for the air material and the high-energy explosive material models are described in details. The results have been validated by comparing FE modelling results of a RC fence under blast detonations with an experimental work, which was performed by others. In the present work, twelve RC fences with two different shapes (Curved and T-Shaped) have been examined against two explosive charges (25 Kg and 50 Kg of TNT). Two different concrete types are used in this paper, Normal Strength Concrete (NSC) and Ultra-High-Performance Concrete (UHPC). The aim of the FE analysis of the twelve models is to study the influence of using the UHPC and the CFRP sheets for improving the blast resistance capacity.*
Results*: The results of the numerical analysis of twelve RC fences have been presented, discussed and were evaluated according to the damage and the value of the deformation.*
Conclusion: *The results of the FE Modelling show that the behaviour of the RC T-shaped fences against blast loads are better than the behaviour of the RC Curved fences, because of the little damage and the low generation of the debris and fragments. Also, the usage of Ultra-High Performance Concrete and the externally bonded CFRP sheets significantly improve the blast resistance capacity of the RC fences.*
Key Word*: Explosion, Blast, RC fences, NSC, UHPC, Fence blast wall, 3D numerical simulation, LS-DYNA, Numerical results, Solid element, Finite element models.*

Date of Submission: 09-06-2020 Date of Acceptance: 26-06-2020

I. Introduction

The increasing in terrorist operations in the world recently, and the enormous loss of human lives caused by explosive incidents, have led to the need to evaluate the behaviour of fences that protect infrastructure and the important buildings against blast loads. Two parameters have a huge influence on the intensity of the explosion; the weight of explosive material and the standoff distance. The fences increase the standoff distance between the source of the explosion and the building, which provide more safety against blast loads.

Various studies have been carried out to improve the explosion resistance of RC elements. Muszynski and Purcell[1] tested a structure consisted of RC walls and columns retrofitted with a carbon fibre-epoxy laminate and biaxial E-glass fabric and subjected to a huge blast load with small standoff distances. They concluded that the pressures caused by the explosion have catastrophic destruction on the structure. The columns failed but the wall didn`t fail but it had suffered large displacements. The carbon-fibre laminate reinforcement performance may be better if it was applied in a continuous sheet rather than strips. Mutalib, Mussa and Hao[2] compared the previous experimental results with numerical results using LS-DYNA Software and there was a good agreement between the experimental results and the numerical results according to displacement and failure shape within an average error of 16%. The study concluded that using CFRP strengthening especially with anchors decreased the damage and increase the capacity of the pressure and impulse under blast loads.

Razaqpur et al.[3] tested RC panels retrofitted with GFRP laminates exposed to various explosive charges. The study concluded that the panels, which retrofitted with GFRP laminates significantly resisted blast loads better than the non-retrofitted panels.

Silva and Lu[4] conducted blast tests on four one-way RC slabs. Two slabs were retrofitted with CFRP covered on one side or both sides, and the other two slabs were retrofitted with steel fibre reinforced polymer laminates covered on one side and both sides also. They concluded that the panels, which covered on both sides significantly resisted blast loads better than the panels, which covered on one side only.

Schenker et al.[5] carried out experimental tests and numerical simulations of four RC slabs exposed to a large explosive charge consisted of 1000 kg hemispherical TNT charge at a stand-off distance equalled 20 m. Two slabs were covered with two or four layers of the aluminium foam, and the other two slabs were uncovered. The study concluded that using the aluminium foams layers provide more protection against blast loads.

Ha et al.[6] carried out field explosion tests on nine protected and unprotected RC panels with explosive charge consisted of 15.88 kg ANFO charge at a standoff distance equalled 1.5 m. RC panels were retrofitted with CFRP layers only, sprayed highly ductile material of polyurea (PU) only and the hybrid CFRP with PU (CPU). The test results showed that CPU had the best performance, the highest energy absorption capacity and the smallest displacement against blast loads.

Tai et al.[7] used the nonlinear finite element analysis program LS-DYNA to discuss the dynamic response and damage pattern of an RC panel exposed to various explosive charges. The study concluded that the mesh size was very effective in blast wave propagation and the accuracy of the results depending on the mesh size. Also, the reinforcement ratio was very effective in deformation. When the reinforcement ratio was very low, the failure occurred at the panel centre, but when it was higher, the deformation decreased and the failure occurred at the supports.

Wang et al.[8] tested six one-way square slabs with different diminutions against several explosive charges. The study concluded that the smaller specimens suffered less damage than the larger specimens. The results showed that there are two main damage shapes, spallation damage from a few cracks, and moderate spallation damage. Wang et al.[9] compared the previous experimental results with numerical results using ANSYS-AUTODYN Software and there was a great agreement between the experimental results and the numerical results.

Pantelides et al.[10] undertook field experiments to predict the performance of five types of RC wall panels against blast loads. The panels' types were Normal Weight Concrete (NWC) with steel bar reinforcement, Fiber Reinforced Concrete (FRC) without reinforcement, FRC with steel bars, NWC with GFRP bars and NWC with steel bars and external biaxial GFRP layers on both sides. The study concluded that the FRC panel with steel bar reinforcement had the best performance against blast loads according to the value of panel deflection, crack width and concrete spalling.

Foglar et al.[11] tested eleven precast RC slabs with a dimension of (0.30 * 1.50 * 6.0 m) retrofitted with waste steel fibres, which were added in the concrete mixture. The explosive charge was 25 kg TNT with a small standoff distance of 0.45 m. The eleven slabs had various compressive strengths ranged from 45 MPa to 82.5 MPa and the fibre density ranged from 4.5 Kg/m3 to 80 Kg/m3. A numerical analysis was carried out using LS-DYNA Software. A great agreement was noticed between the experimental results and the numerical results. The RC slab with a compressive strength of 65 MPa and a fibre density of 80 Kg/m3 had the best performance and the lowest damage in comparison with other RC slabs.

Alsayed et al.[12] conducted blast tests on ten infill masonry walls strengthened and unstrengthened with two layers of GFRP sheets on the back face. The explosive charges were varying from 1.1 kg C4 to 500 Kg C4 with standoff distances varying from 2 m to 4.8 m. A numerical analysis was carried out using ANSYS-AUTODYN Software. The results showed that there was a great agreement between the experimental results and the numerical results. The numerical analysis was able to predict the failure modes, blast pressures and damage patterns with reasonable accuracy. The study concluded that the most effective parameter for increasing the level of damage of blast loads was standoff distance. Test results showed that using GFRP layers with suitable end anchorage resisted low to medium blast loads and reduced the fragments.

G. Mahmoud et al.[13] carried out numerical analysis using ANSYS-AUTODYN Software on six panels with explosive charge equalled 50 Kg TNT with a standoff distance 1 m. The six panels consisted of two steel plates with a 0.35 m gap. The first two panels were two steel plates with a thickness of 5 mm or 20 mm filled with air. The other two panels were the same as the previous but filled with normal concrete. The last two panels were two steel plates with thickness 20 mm connected by shear connectors distributed horizontally or horizontal plates distributed

vertically. The finding of the study revealed that the thickness of the plates had a significant effect on the panel deformation, and filling the gap between plats with normal concrete decreased the deformation with comparing to the air-filling panel. The study also concluded that the shear connectors and the horizontal plates improved the performance of the panels against blast loads and reduced the plastic zone without any failure in the panels.

Syed et al.[14] carried out numerical simulations of one-way RC panels exposed to explosive charges varying from 0.5 kg to 1000 Kg TNT with a standoff distance varying from 0.25 m to 41 m using LS-DYNA Software to investigate the relation between the incident angle value, shock density and the failure modes. The study concluded that blast waves with shock density less than 3.5 kg/m^3 caused a flexural failure, but shock densities more than that value caused localised failures.

Adhikary et al.[15] undertook field experiments on five RC panels strengthened and unstrengthened with strain-hardening cementitious composite (SHCC) layers under explosive charge equalled 5 Kg TNT with standoff distance equalled 1 m. The first RC panel was unstrengthened and considered as a control panel. The other panels were strengthened on one side or both sides with the SHCC layer varying in thickness. A numerical analysis was carried out using LS-DYNA Software and the results compared with experimental results. A great agreement was noticed between the experimental results and the numerical results. The finding of the study revealed that SHCC layers improved the performance of the RC panel with comparing with the control panel. The performance of the RC panel may be better if SHCC layers were applied on both sides rather than on one side.

Jin, Hao and Hao [16] carried out numerical simulations using ANSYS-AUTODYN Software on steel fences were previously field-tested in (Hao et al., 2017)[17] under blast loads. The fences consisted of circular or triangular steel poles with a different number of layers exposed to explosive charge equalled 1.0 kg TNT with several standoff distances. The study concluded that decreasing the gap between steel poles and increasing the number of layers would increase the performance of the fence in resisting blast loads, but it would lead to a huge cost. The triangular steel poles were more effective than circular steel poles because the triangular`s shape had the ability of distracting blast waves.

Xiao, Andrae and Gebbeken[18] and Xiao et al.[19] conducted field tests on three walls against blast loads. The first wall consisted of a gabion wall only, but the second one consisted of a gabion wall with a steel canopy mounted at the top of it with an angel equalled 45° and 135° for the third wall. A numerical analysis was carried out using LS-DYNA Software and the results compared with experimental results. A great agreement was noticed between the experimental results and the numerical results. The finding of the study revealed that the canopies could reduce blast intensity behind the gabion wall, and the third wall had the best performance in that.

In the present paper, a numerical study for evaluating the behaviour of the RC Curved and T-Shaped fences against blast loads has been carried out and the results were evaluated according to the value of the deformation. The results have been validated by comparing FE modelling results of a RC fence under blast detonations with an experimental work, which was performed by Pantelides et al.[10]. Twelve RC fences with two different shapes (Curved and T-Shaped) have been examined against two explosive charges (25Kg and 50Kg of TNT). Two different concrete types are used in this paper, Normal Strength Concrete (NSC) and Ultra-High-Performance Concrete (UHPC). Our goal here, therefore, is to evaluate the behaviour of the RC Curved and T-Shaped fences against blast loads to reach to the best case of the FE models that can resist a high blast load and protect the important buildings very well.

II. Explosion Phenomena

Definition of explosion: An explosion is defined as a sudden and rapid release of energy in the form of sound, heat, light and a shock wave [20].

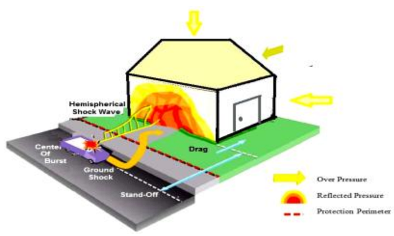

Figure 1: hemispherical shock wave due to a vehicle blast**.**

Types of blast waves:

1. **Shock waves:**

In this type of blast wave, the pressure rises suddenly and instantaneously from the ambient atmospheric magnitude (Po) to an incident-free field overpressure (Pso). This incident-free field overpressure (P_{SO}) returns to the ambient atmospheric magnitude (Po) again with highly damped pressure reversals. This leads to a negative (suction) phase that follows the positive phase of the blast wave. The negative phase of a shock or pressure wave is usually much weaker and more gradual than the positive phase.

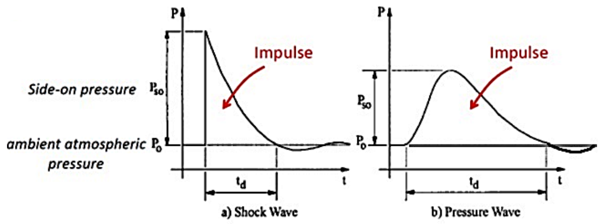

Figure 2: Types of blast waves [21].

2. Pressure waves:

As shown in Figure 2, the pressure rises gradually to the peak overpressure and then the pressure decreases gradually and a negative (suction) phase occurs similar to that for the shock wave.

Peak Reflected Pressure (Pr):

When blast wave strikes a solid surface, which inclines at a specific angle to the direction of the flow of blast wave, it is reflected on the surface. The value of the peak reflected pressure (Pr) depends on both the value of (Pso) and the angle between the direction of the blast wave and the surface. The reflected pressure reaches its maximum value when the surface is perpendicular to the direction of blast wave (The slope angle of blast wave $\{\alpha\} = 0°$). It reaches its small value the surface is parallel to the direction of blast wave (The slope angle of blast wave $\{\alpha\} = 90°$) [21].

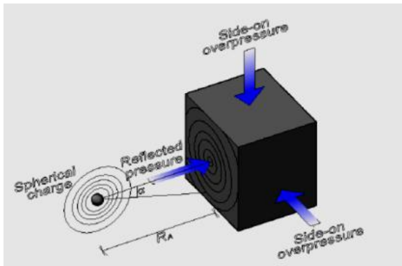

Figure 3: Reflected pressure acting on a cube building.

The peak reflected pressure (Pr) can be determined from [22]:

$$Pr = Cr\alpha \cdot Pso \qquad \text{Eq. 1}$$

where: Crα: Coefficient of reflection.
Pso: perusserprevo evitisop tnedicni kae.

This coefficient of reflection depends on the value of p tnedicni kae erusserprevo evitisop (Pso), the angle between the direction of the blast wave and the surface and on the characteristics of the blast wave itself.

III. Reinforced concrete fences:

The reinforced concrete fences can be divided with respect to mobility into two main types: Fixed and Movable reinforced concrete fences.

Fixed reinforced concrete fence:

It`s a cast-in-place reinforced concrete structure, it`s consists of plain and reinforced concrete footing under the ground surface level and then a reinforced concrete wall with a specific thickness and height resulting from its design against blast loads. Figure 4 shows the Fixed reinforced concrete fences.

Movable reinforced concrete fences:

It`s a precast reinforced concrete fence, it`s formed of units of 5 to 10 tons that are moved by a huge crane. They are placed in front of the building that needed to be protected against blast loads and they can be taken away and used anywhere.

There are two common types of movable RC fences in Egypt, RC Curved fences and RC T-Shaped fences, which can be used to provide the protection for important buildings against blast loads. Figure 5 shows the movable reinforced concrete fences, while Figure 6 shows the dimensions of the RC Curved and T-Shaped fences. The reinforcement details of the RC Curved and T-Shaped fences are shown in Figure 7.

IV. The problem statement

In the case of the RC Curved fence, the angle between the direction of the blast wave and the surface is very close to equal 90° in all points on the surface. When a blast wave is perpendicular to the surface (The slope angle of blast wave {α} =0°), the reflected pressure is at its maximum value. This problem makes the RC Curved fence very weak to resist blast loads.

In the case of the RC T-Shaped fence, the angle between the direction of the blast wave and the surface isn`t equal 90° in all points on the surface except the bottom zone, which has a larger concrete thickness than the top zone. The reflected pressure value on the case of the RC T-Shaped fence is smaller than its value in the case of the RC Curved fence.

Figure 8 shows the distribution of blast waves on the surface of the RC Curved and T-Shaped fences. A numerical analysis will carry out to investigate deeply the behaviour of the RC Curved and T-Shaped fences against blast loads.

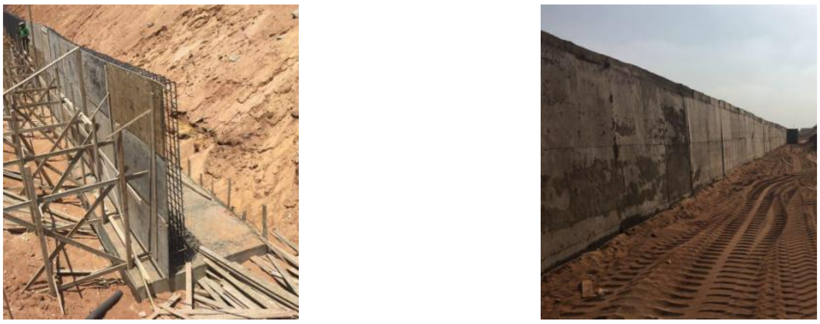

Figure 4: Fixed reinforced concrete fence.

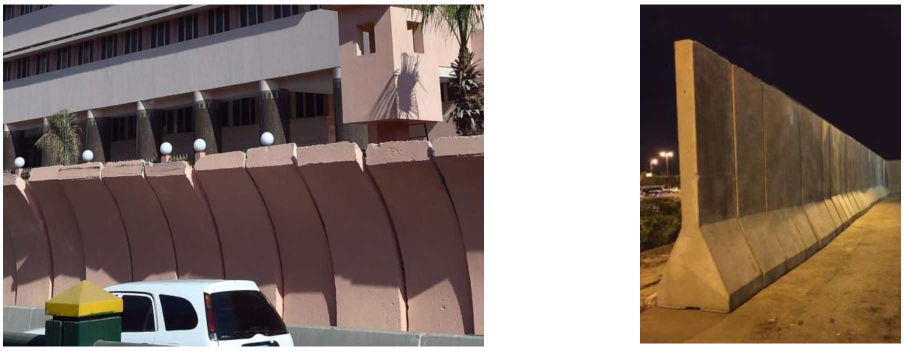

Figure 5: The RC Curved and T-Shaped fences**.**

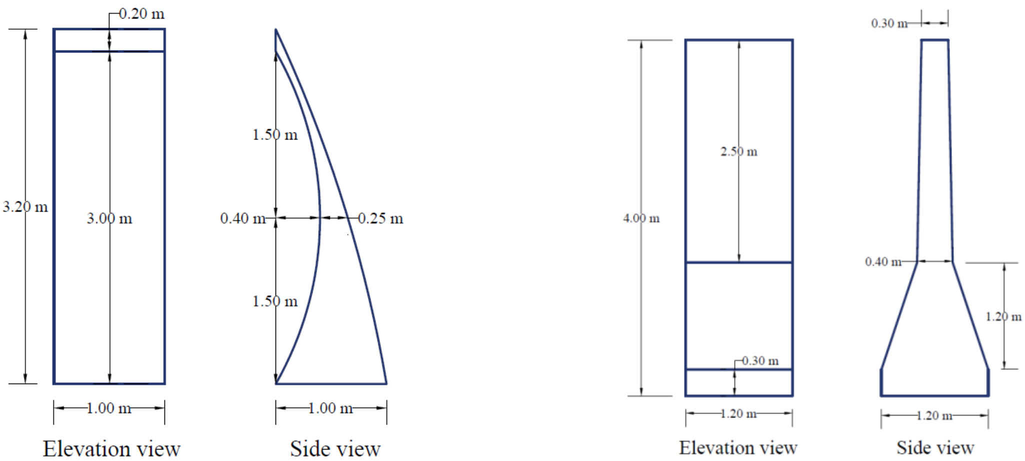

Figure 6: The dimensions of the fences.

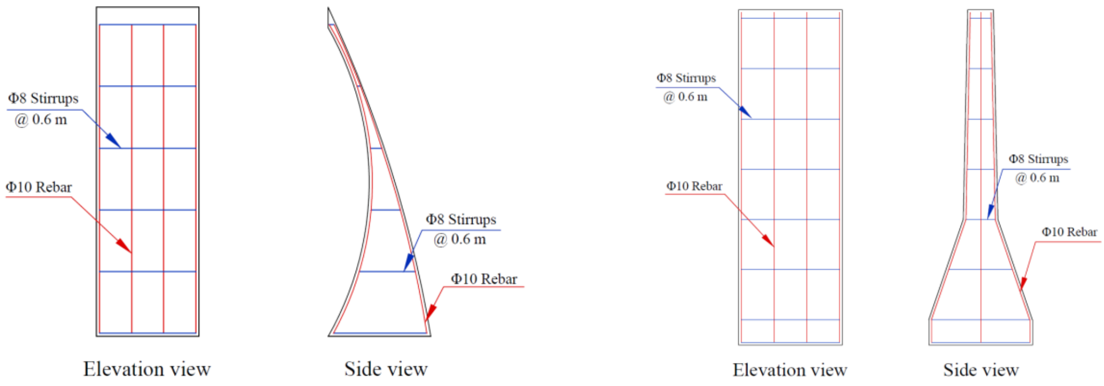

Figure 7: The reinforcement detailing of the fences.

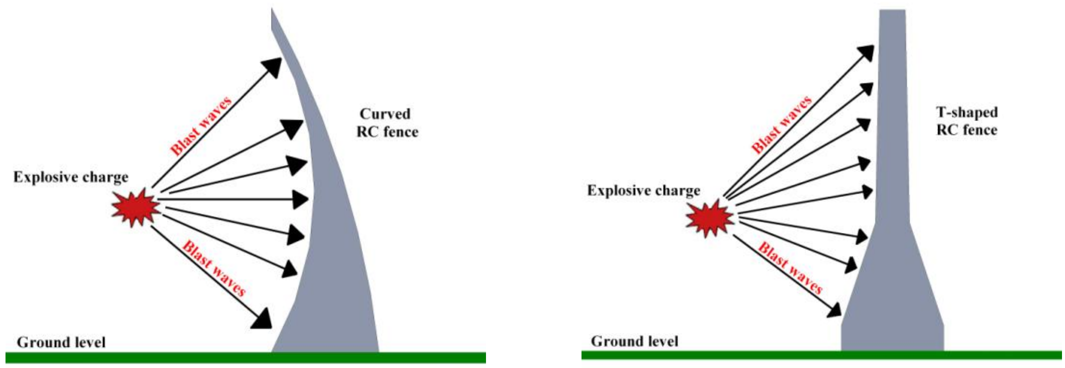

Figure 8: Blast waves distribution on the RC Curved and T-Shaped fences.

V. Finite Element modelling using LS-DYNA

LS-DYNA is a general-purpose finite element code for analyzing the large deformation dynamic response of structures [23]. The main solution methodology is based on explicit time integration. LS-DYNA currently contains approximately one-hundred constitutive models and ten equations-of-state to cover a wide range of the behaviour of the materials. Agardh[24] and Leppänen[25] had widely validated LS-DYNA Software against results of experimental tests.

In the present study, the material behaviour in the numerical simulations is described by the partial differential equations with Equations of State (EOS) and constitutive models. In addition to the previous, a set of initial and boundary conditions define the complete system for blast simulations. This analysis is carried out using the commercial program LS-DYNA. The partial differential equations are used to govern the basic physics principles of conservation of mass, momentum, and energy.

Material and Equation of state of models:

1. Air Modelling:

Air is modelled with 8-node finite elements using the (MAT_NULL) material model with the hourglass coefficient equals ($1*10^{-6}$). The air modelling parameters are shown in Table 1. The equation of state for air is modelled by using the linear polynomial equation of state [23]:

$$p = C_0 + C_1 \mu + C_2 \mu^2 + C_3 \mu^3 + E(C_4 + C_5 \mu + C_6 \mu^2) \quad \text{Eq. 2}$$

For an ideal gas, this equation can be reduced using appropriate coefficients:

($C_0 = C_1 = C_2 = C_3 = C_6 = 0$, $C_4 = C_5 = (\gamma - 1)$), Where: $\mu = \frac{\rho}{\rho_0} - 1$

Eq. 3

So: $p = (\gamma - 1)\frac{\rho}{\rho_0} - 1$

Eq. 4

Where ρ_0 and ρ are the initial and actual densities of air, and E is the specific internal energy with units of pressure and γ is the adiabatic expansion coefficient.

Table 1: The air modelling parameters [7,26].

Symbol	Mean	Value
R0	Mass Density	1.293 (Kg/m^3)
C0,C1,C2,C3 and C6	The polynomial equation coefficients	0
C4 and C5	The polynomial equation coefficients	0.40
E0	Initial internal energy per unit volume	2.50*10^5 (Pa)
V0	Initial relative volume	1.00
γ	the adiabatic expansion coefficient for air	1.40

2. Explosion Modelling:

The TNT material is modelled with 8-node finite elements using the (MAT_HIGH_EXPLOSIVE_BURN) material model with the command (INITIAL_DETONATION) [27]. The TNT material modelling parameters are shown in Table 2. The equation of state for the explosion is modelled by using the JWL High Explosive Equation of state.

The JWL equation of state defines pressure as a function of relative volume, V, and internal energy per initial volume, E, as:

$$P = C_1\left(1 - \frac{\omega}{r_1 v}\right)e^{-r_1 v} + C_2\left(1 - \frac{\omega}{r_2 v}\right)e^{-r_2 v} + \frac{\omega e}{v}$$

Eq. 5

where C_1, C_2, r_1 and r_2 are constants and e, ω and v are the internal energy, the adiabatic constant and the specific volume, respectively [23].

Table 2: The TNT material modelling parameters [28,29].

Symbol	Mean	Value
R0	Mass Density	1630 (Kg/m3)
D	Detonation velocity	6930 (m/s)
PCJ	C-J Pressure	2.10*10^{10} (Pa)
A	Parameter , C1	3.712*10^{11} (Pa)
B	Parameter, C2	3.231*10^9 (Pa)
R1	Parameter	4.15
R2	Parameter	0.95
OMEGA	Parameter	0.30
E0	Initial internal energy per unit volume	7.00*10^9 (Pa)
V0	Initial relative volume	1.0

3. Concrete Modelling:

LS-DYNA Software contains many material models that can be used to modelling the concrete. The Winfrith concrete model (WCM) and the Concrete Damage Release 3 model (CMR3M) describe the plastic behaviour of the material, include strain rate effects and are able to predict the local and global response of concrete elements exposed to the explosive loads [30].

Vasudevan[31] compared experimental results with numerical results using LS-DYNA Software on RC slabs using the WCM and the CMR3M under blast loads and concluded that the WCM provided a better response in terms of deflection and crack propagation than the CMR3M. In the present study, the WCM is chosen to modelling the concrete of the RC fences.

The WCM is a smeared crack model that is implemented in 8-node single integration point continuum elements [32]. The strain-rate effects are taken into consideration in the WCM by setting the value of (RATE) in the material card to equal zero [32]. Figure 9 shows the stress-strain curve of a unit cube element using the WCM exposed to a uniaxial loading [30].

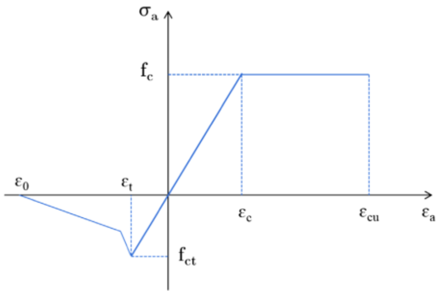

Figure 9: Stress-Strain curve for the WCM exposed to uniaxial loading.

The command (CONSTRAINED_LAGRANGE_IN_SOLID) is used to model the interaction between the blast loads in the air and the concrete [33]. The erosion isn`t taken into consideration in the WCM until using the additional command (MAT_ADD_EROSION). NSC and UHPC modelling parameters are listed in Table 3.

Table 3: NSC and UHPC modelling parameters [10,34].

Symbol	Mean	NSC	UHPC
R0	Mass Density	2500 (Kg/m^3)	2500 (Kg/m^3)
TM	Initial Tangent Modulus of Concrete	$30*10^9$ (Pa)	$56.242*10^9$ (Pa)
PR	Poisson`s Ratio	0.20	0.20
UCS	Uniaxial Compressive strength	$51*10^6$ (Pa)	$182.8*10^6$ (Pa)
UTS	Uniaxial tensile strength	$4*10^6$ (Pa)	$9.50*10^6$ (Pa)
ASIZE	Max Aggregate size	0.01 m	0.008 m
EPSP1	Maximum principle strain at failure	0.023	0.096

4. Reinforcement Steel Modelling:

The reinforcement steel material is modelled as beam elements with Hughes-Liu formulation using the (MAT_PLASTIC_KINEMATIC) material model [33]. The reinforcement Steel modelling parameters are listed below in Table 4.

Table 4: The reinforcement Steel modelling parameters [33].

Symbol	Mean	Value
R0	Mass Density	7850 (Kg/m3)
E	Young's modulus of steel	$2.00*10^{11}$ (Pa)
PR	Poisson's ratio	0.30
SIGY	Yield stress of steel	$4.20*10^8$ (Pa)
FS	Failure strain for eroding elements	0.25

5. CFRP Modelling:

The CFRP sheets are modelled using 4-node shell elements with the Belytschko-Tsay formulation using the (*MAT_ENHANCED_COMPOSITE_DAMAGE) material model, this material model is an orthotropic material with optional brittle failure. The failure criterion of Chang and Chang [35] is used to define the failure of CFRP sheets. The CFRP shell elements consist of four layers of CFRP sheets with a thickness of 1.00 mm for each sheet.

The command (CONTACT_TIEBREAK_SURFACE_TO_SURFACE) is used to model the bond between the CFRP sheets and the RC concrete. The RC concrete elements are defined as the master surface, while the CFRP shell elements are defined as the slave surface. The tiebreak contact modelling has been validated earlier in other works by Elsanadedy et al.[36], Elsanadedy et al.[37], Almusallam, Elsanadedy and Al-Salloum[38] and Almusallam et al.[39].

Tiebreak contact allows the separation of the tied surfaces under tensile and shear loads using the following an interface strength-based failure criterion:

$$\left(\frac{|\sigma_n|}{NFLS}\right)^2+\left(\frac{|\sigma_s|}{SFLS}\right)^2\geq 1 \qquad \text{Eq. 6}$$

where, σ_n: the normal stress, σ_s: the shear stress, NFLS: the tensile failure stress and SFLS: the shear failure stress.

The following equations were proposed by Lu et al.[40] to estimate NFLS and SFLS values and then validated by Lu et al.[41]:

$$NFLS = 0.395 f_{cu}^{0.55} = 0.447 (f_c^{\prime})^{0.55}$$ Eq. 7

where f_{cu}: the concrete cube compressive strength (MPa) and $f`_c$: the concrete cylinder strength (MPa). The concrete cylinder strengths values of the NSC and the UHPC are 51 (MPa) and 182.8 (MPa), respectively.

$$SFLS = 1.5 \beta_w NFLS$$ Eq. 8

where, β_w: the CFRP-to-RC concrete width ratio factor, which affects the bond-slip parameters, and it is given by:

$$\beta_w = \sqrt{\frac{2.25 - b_f/b_c}{1.25 + b_f/b_c}}$$ Eq. 9

where b_c: the width of the RC fence and b_f: the width of the CFRP sheet. The CFRP modelling parameters are listed below in Table 5.

6. Ground Surface Modelling:

The ground surface is modelled as a rigid concrete plate using the (MAT_RIGD) material model. Table 6 shows the rigid plate material modelling parameters. The contact between the fences and the rigid plate is modelled using (CONTACT_AUTOMATIC_SURFACE_TO_SURFACE) contact option, the fences are defined as the slave part, while the rigid plate elements are defined as the master part. The hinged supported boundary conditions are applied to the bottom nodes of the rigid plate; the translation in the three dimensions is restricted.

Table 5: The CFRP modelling parameters [37,42].

Symbol	Mean	Value
R0	Mass Density	1600 (Kg/m3)
EA	Longitudinal Young's modulus	$1.27*10^{11}$ (Pa)
EB	Transverse Young's modulus	$1.70*10^{10}$ (Pa)
PR	Poisson's ratio	0.30
G	Shear modulus	$6.00*10^{9}$ (Pa)
XC	Longitudinal compressive strength	$1.20*10^{9}$ (Pa)
XT	Longitudinal tensile strength	$1.50*10^{9}$ (Pa)
YC	Transverse compressive strength	$2.50*10^{8}$ (Pa)
YT	Transverse tensile strength	$5.00*10^{7}$ (Pa)
SC	Shear strength	$7.00*10^{7}$ (Pa)
NFLS	Tensile failure stress in case of contacting with NCS	3885716.58 (Pa)
	Tensile failure stress in case of contacting with UHPC	7841414.81 (Pa)
SFLS	Shear failure stress in case of contacting with NCS	4344363.25 (Pa)
	Shear failure stress in case of contacting with UHPC	8766968.36 (Pa)

Table 6: The rigid plate modelling parameters.

Symbol	Mean	Value
R0	Mass Density	2500 (Kg/m^3)
E	Young's modulus	$2.1*10^{11}$ (Pa)
PR	Poisson`s Ratio	0.20

VI. Verification model

Experimental test:

Tests of the RC wall conducted by Pantelides et al.[10] are used for validation of the FE models. The test specimen was (1.2 m * 1.2 m) RC wall constructed using Normal Strength Concrete (NSC) and the thickness was 152 mm. The NSC had an average static 28-day compressive strength of 51 MPa and an average static tensile strength of 4.0 MPa. The explosive charge was 6.2 Kg TNT. The standoff distance was 1.0 m and the charge was located at the mid-height of the wall. The wall was placed on the ground and large concrete blocks were placed on each side of the wall to provide support, as shown in Figure 10.

The nominal tensile strength of the steel rebars was 420 MPa and the modulus of elasticity was 200 GPa. The wall was reinforced with 10 mm diameter steel bars spaced at 305 mm, as shown in Figure 11.

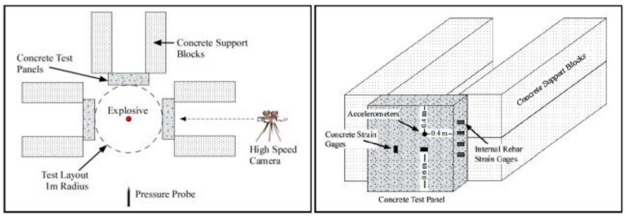

Figure 10: The experimental setup of the RC wall**.**

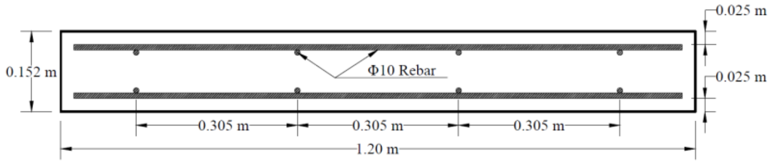

Figure 11: The reinforcement detailing of the RC wall.

FE Modelling:

The Air Modelling, the Explosion Modelling, the Concrete Modelling and the Reinforcement Steel Modelling have been explained previously in section (Material and Equation of state of models).
The ground surface and the rigid supports is modelled as a rigid concrete using the (MAT_RIGD) material model, as explained previously in section (Ground Surface Modelling).

The contact between the wall and the rigid parts is modelled using (CONTACT_AUTOMATIC _SURFACE_TO_SURFACE) contact option, the wall is defined as the slave part, while the rigid parts are defined as the master part. The hinged supported boundary conditions are applied to the bottom nodes of the rigid parts; the translation in the three dimensions is restricted.

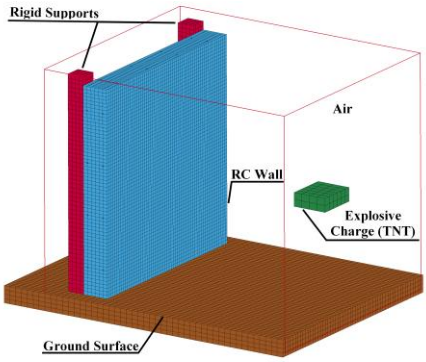

Figure 12: The FE model of the RC wall.

Results:

Table 7 compares the maximum deflection of the RC wall measured from the experimental test and the FE analysis results. It shows that FE analysis results agree well with the test results. The difference between the experimental test and the FE analysis results is 0.428%. The maximum deflection of the RC wall measured from the FE analysis results is shown in Figure 13.

Table 7: Comparison of maximum deflection of the RC wall.

Specimen	Test Results (m)	FE Results (m)	Difference
RC Wall	0.082	0.082351	0.428 %

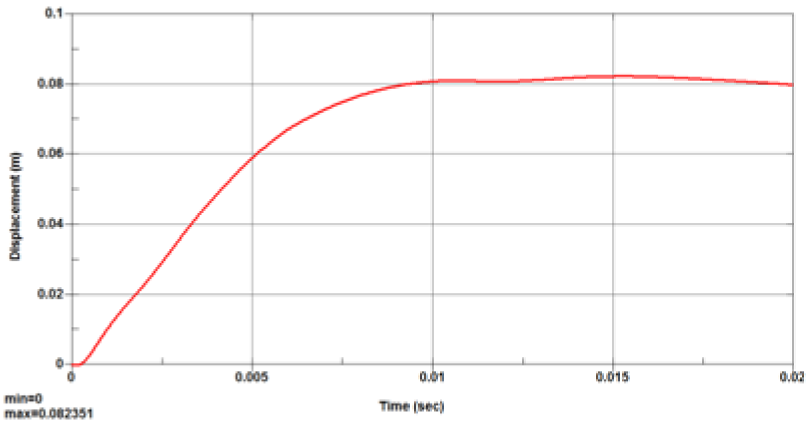

Figure 13: The maximum deflection of the RC wall measured from the FE analysis results.

In addition to the previous comparison, a comparison of damage of the RC wall between the experimental test and the FE analysis results is shown in Figure 14. The comparison shows that the damage of the RC wall resulted from the FE analysis method agrees well with that of the experiment.

In conclusion, the developed FE model accurately predicted the deflection and damage of the RC wall against blast loads.

(a)

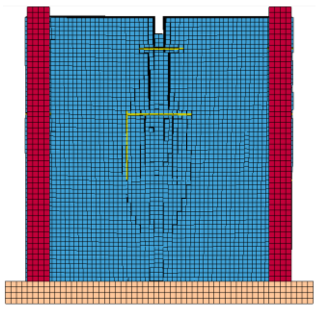

(b)

(c)

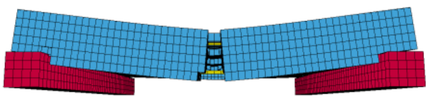

(d)

Figure 14: Comparison of damage of the RC wall,
(a) and (c) The back and the top view from experimental results by Pantelides et al.[10].
(b) and (d) The back and the top view from FE analysis results.

VII. FE Modelling Applications

Twelve RC fences with two different shapes have been examined against two explosive charges with fixed standoff distances equal 2.00 m and the height of the explosive charge is 1.25 m from the ground surface.
The aim of the FE analysis of the twelve models is to study the influence of using the UHPC and the CFRP sheets against blast loads.
Table 8 summarizes the FE analysis of the twelve models.

The Deflection Measurements:

For the RC Curved fences, the deflections are measured at time 0.10 sec at three points A, B and C at levels 0.0, 1.50 m and 3.00 m, respectively.

But in the case of the RC T-Shaped fences, the deflections are measured at time 0.10 sec at four points A, B, C and D at levels 0.0, 1.50 m, 3.00 m and 4.00 m, respectively. The deflection gauges of the RC Curved and T-Shaped fences is shown in Figure 15.

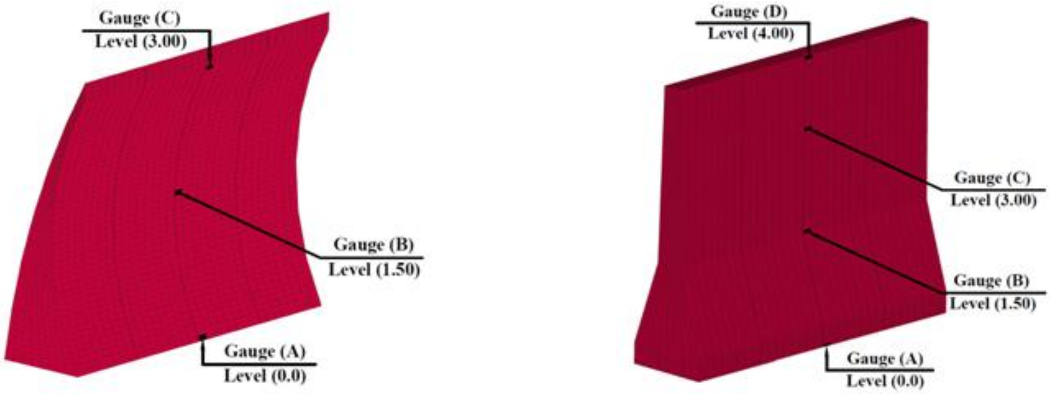

Figure 15: The deflection gauges of the RC Curved and T-Shaped fences.

Table 8: Summary of the FE analysis of the twelve models.

Explosive charge (TNT)	**The shape of the fence**	**Type of the Concrete**	**Retrofitting with CFRP sheets**	**Model ID**
25 KG	Curved fence	Normal Strength Concrete	No	NSC_C25
			4 layers of CFRP sheets	NSC_C25_CFRP
		Ultra-High Performance Concrete	No	UHPC_C25
	T-Shaped fence	Normal Strength Concrete	No	NSC_T25
			4 layers of CFRP sheets	NSC_T25_CFRP
		Ultra-High Performance Concrete	No	UHPC_T25
50 KG	Curved fence	Normal Strength Concrete	No	NSC_C50
			4 layers of CFRP sheets	NSC_C50_CFRP
		Ultra-High Performance Concrete	No	UHPC_C50
	T-Shaped fence	Normal Strength Concrete	No	NSC_T50
			4 layers of CFRP sheets	NSC_T50_CFRP
		Ultra-High Performance Concrete	No	UHPC_T50

RC fences exposed to 25 Kg of TNT explosive charge:

Six FE models consist of three RC Curved fences with two different concrete material types (NSC and UHPC) and three RC T-Shaped fences with two different concrete material types (NSC and UHPC) exposed to blast loads of an explosive charge of 25 Kg of TNT explosive material. The deflections and the damages of the fences are measured.

a) The Deflections:

In the case of The (NSC_C25 and NSC_C25_CFRP) fences, the deflections are measured at a time of 0.10 sec at Gauge A only because the concrete at Gauge B and Gauge C is collapsed. For the other fences, the deflections are measured at a time of 0.10 sec at all Gauges. Table 9 shows the deflections values of the fences due to 25 Kg of TNT at time 0.1 sec. The displacement curves of the fences due to 25 Kg of TNT at time 0.1 sec are shown in Figure 16.

Table 9: The deflections values of the fences due to 25 Kg TNT at time 0.1 sec.

Model ID	Deflection Values (m)			
	Gauge A	Gauge B	Gauge C	Gauge D
NSC_C25	0.4449	can`t be measured	can`t be measured	------
NSC_C25_CFRP	0.1983	can`t be measured	can`t be measured	------
UHPC_C25	0.0491	0.4485	0.7993	------
NSC_T25	0.2734	0.5841	0.8917	1.1008
NSC_T25_CFRP	0.2771	0.5786	0.8725	1.0731
UHPC_T25	0.0593	0.1351	0.2078	0.2582

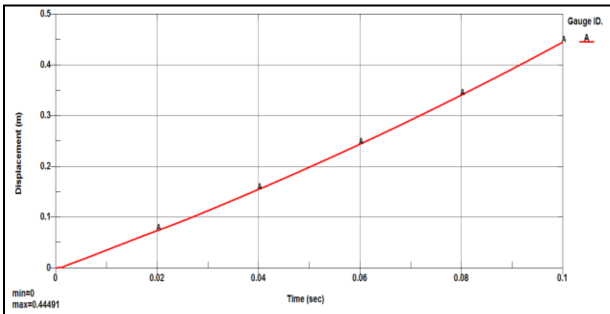

NSC_C25

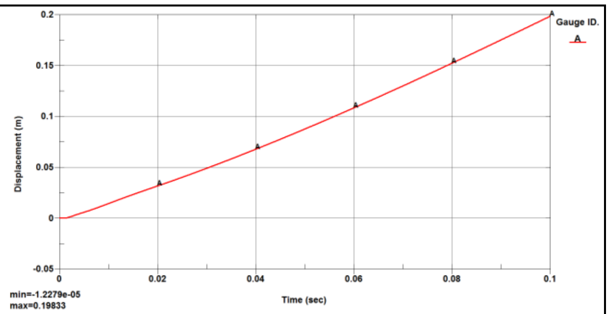

NSC_C25_CFRP

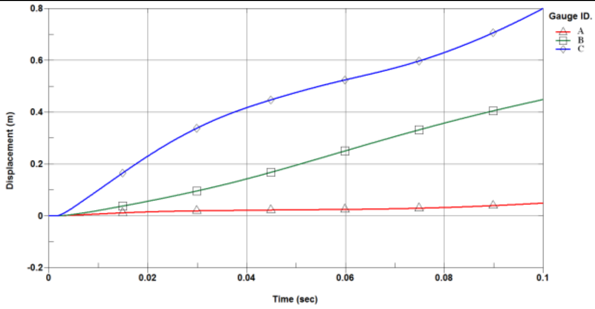

UHPC_C25

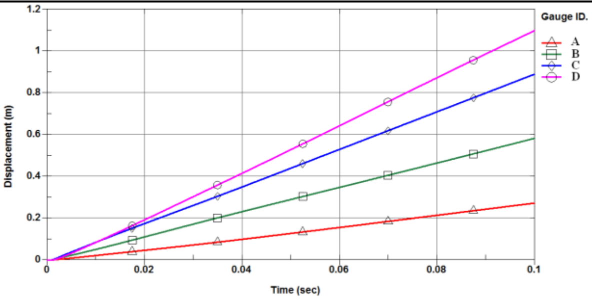

NSC_T25

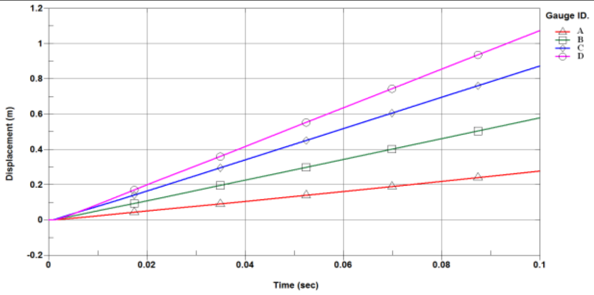

NSC_T25_CFRP

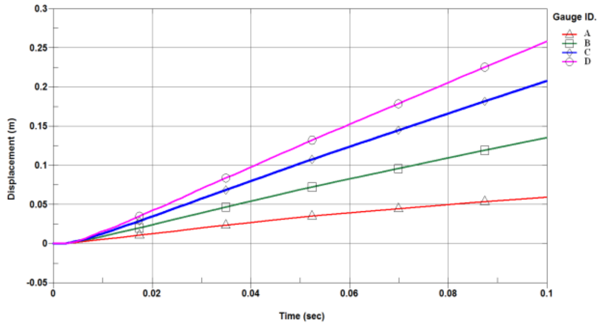

UHPC_T25

Figure 16: The displacement curves of the fences due to 25 Kg at time 0.1 sec.

b) The Damage:

Figure 17 and Figure 18 show a comparison between the damage of the fences due to 25 Kg of TNT at time 0.1 sec.

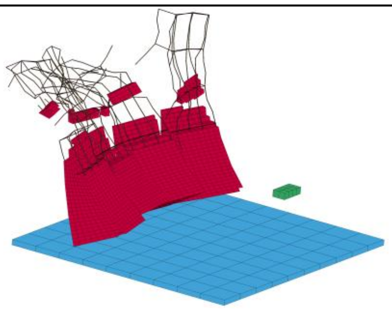

NSC_C25

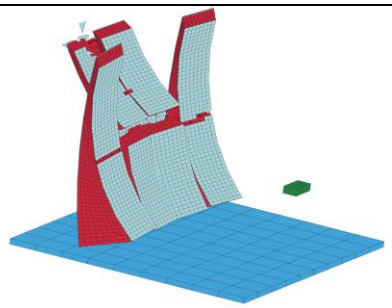

NSC_C25_CFRP

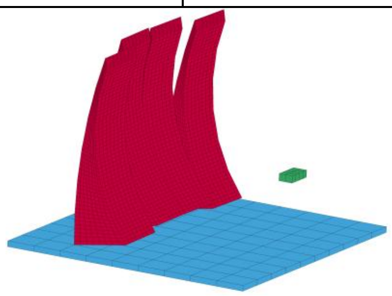

UHPC_C25

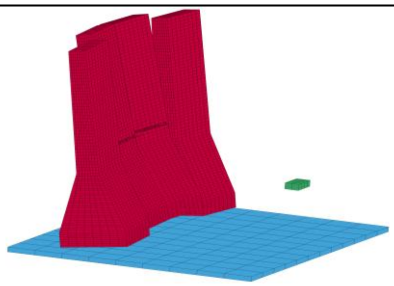

NSC_T25

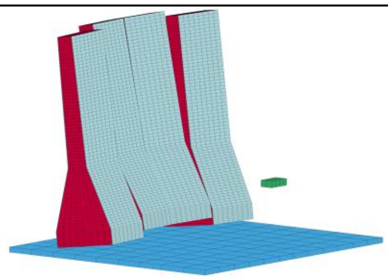

NSC_T25_CFRP

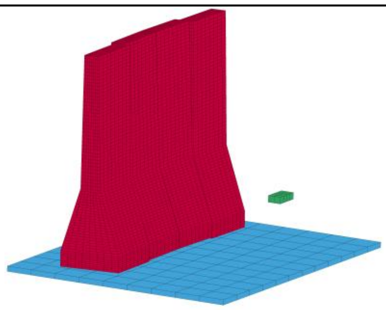

UHPC_T25

Figure 17: The damage of the fences due to 25 Kg at time 0.10 sec. (3D View)

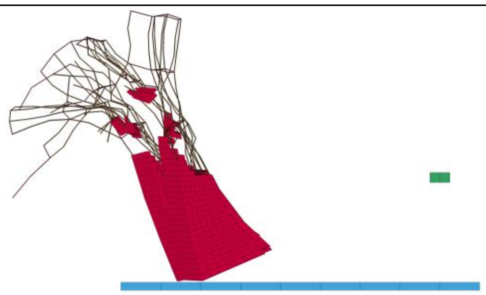

NSC_C25

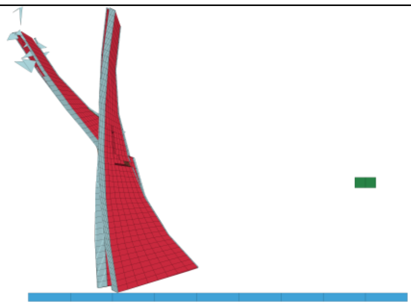

NSC_C25_CFRP

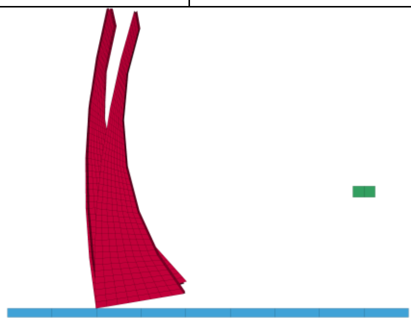

UHPC_C25

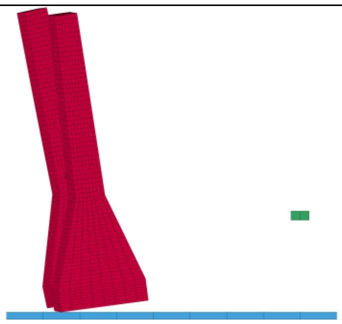

NSC_T25

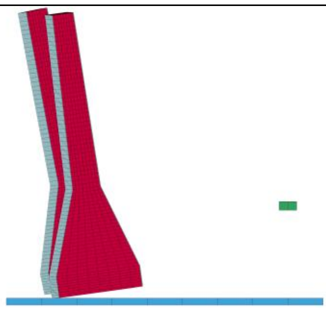

NSC_T25_CFRP

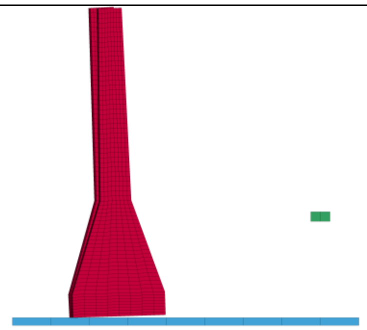

Figure 18: The damage of the fences due to 25 Kg at time 0.10 sec. (Side View)

RC fences exposed to 50 Kg of TNT explosive charge:

Six FE models consist of three RC Curved fences with two different concrete material types (NSC and UHPC) and three RC T-Shaped fences with two different concrete material types (NSC and UHPC) exposed to blast loads of an explosive charge of 50 Kg of TNT explosive material. The deflections and the damages of the fences are measured.

a) The Deflections:

In the case of The (NSC_C50 and NSC_C50_CFRP) fences, the deflections are measured at a time of 0.10 sec at Gauge A only because the concrete at Gauge B and Gauge C is collapsed. For the (UHPC_C50) fence, the deflections are measured at a time of 0.10 sec at Gauge A and Gauge B only because the concrete at Gauge C is collapsed. But in the other fences, the deflections are measured at a time of 0.10 sec at all Gauges. Table 10 shows the deflections values of the fences due to 50 Kg of TNT at time 0.1 sec. The displacement curves of the fences due to 50 Kg of TNT at time 0.1 sec are shown in Figure 19.

Table 10: The deflections values of the fences due to 50 Kg TNT at time 0.1 sec.

Model ID	Deflection Values (m)			
	Gauge A	Gauge B	Gauge B	Gauge D
NSC_C50	0.6070	can`t be measured	can`t be measured	------
NSC_C50_CFRP	0.3343	can`t be measured	can`t be measured	------
UHPC_C50	0.1083	0.6728	can`t be measured	------
NSC_T50	0.4183	0.8153	1.2341	1.5244
NSC_T50_CFRP	0.4146	0.8165	1.2104	1.4752
UHPC_T50	0.1006	0.2170	0.3287	0.4061

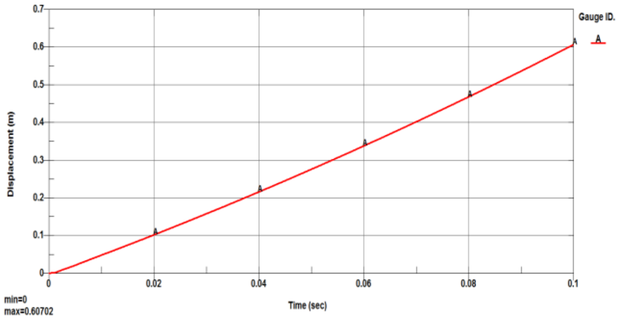

NSC_C50

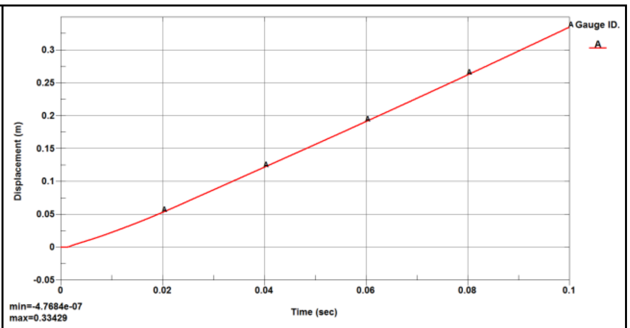

NSC_C50_CFRP

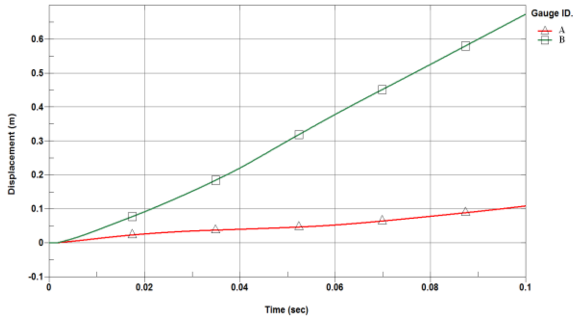

UHPC_C50

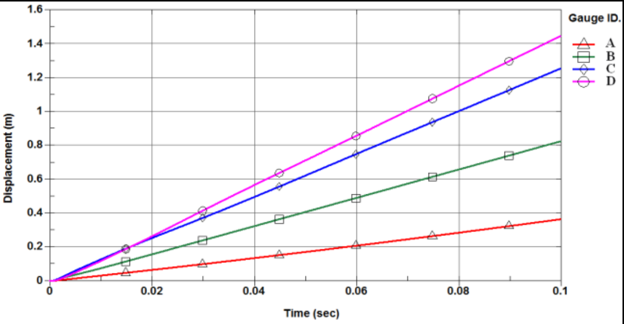

NSC_T50

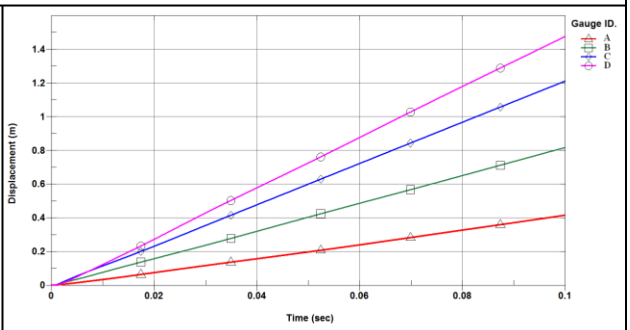

NSC_T50_CFRP

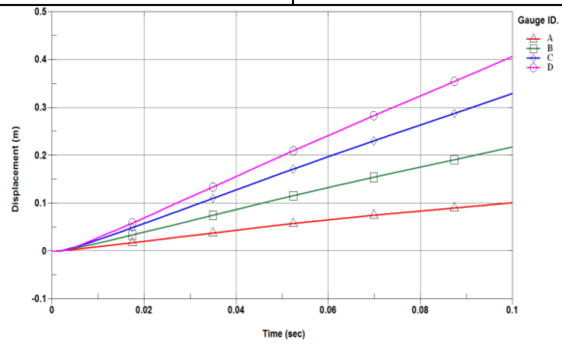

UHPC_T50

Figure 19: The displacement curves of the fences due to 50 Kg at time 0.1 sec.

b) The Damage:

Figure 20 and Figure 21 show a comparison between the damage of the fences due to 50 Kg of TNT at time 0.1 sec.

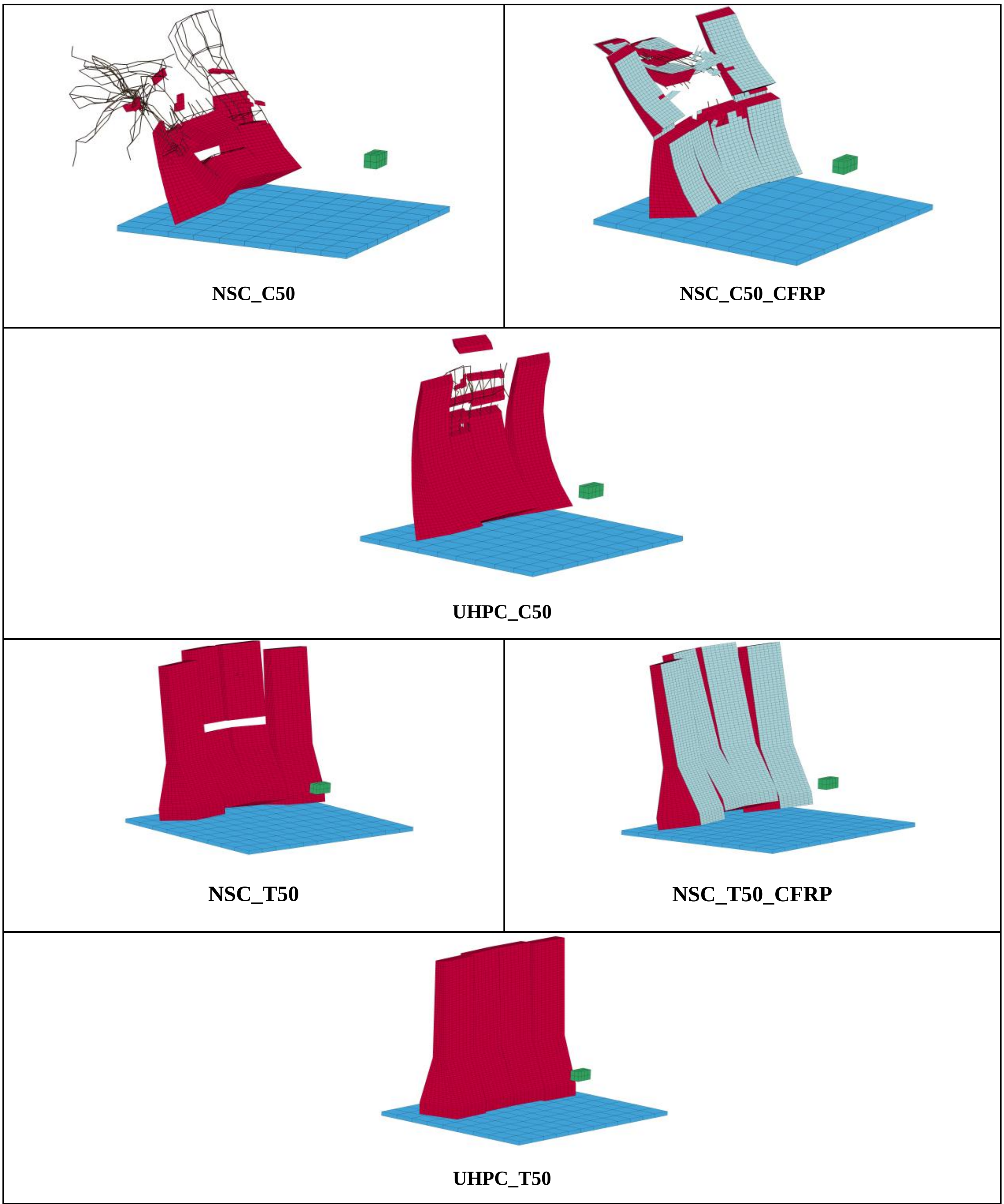

Figure 20: The damage of the fences due to 50 Kg at time 0.10 sec. (3D View)

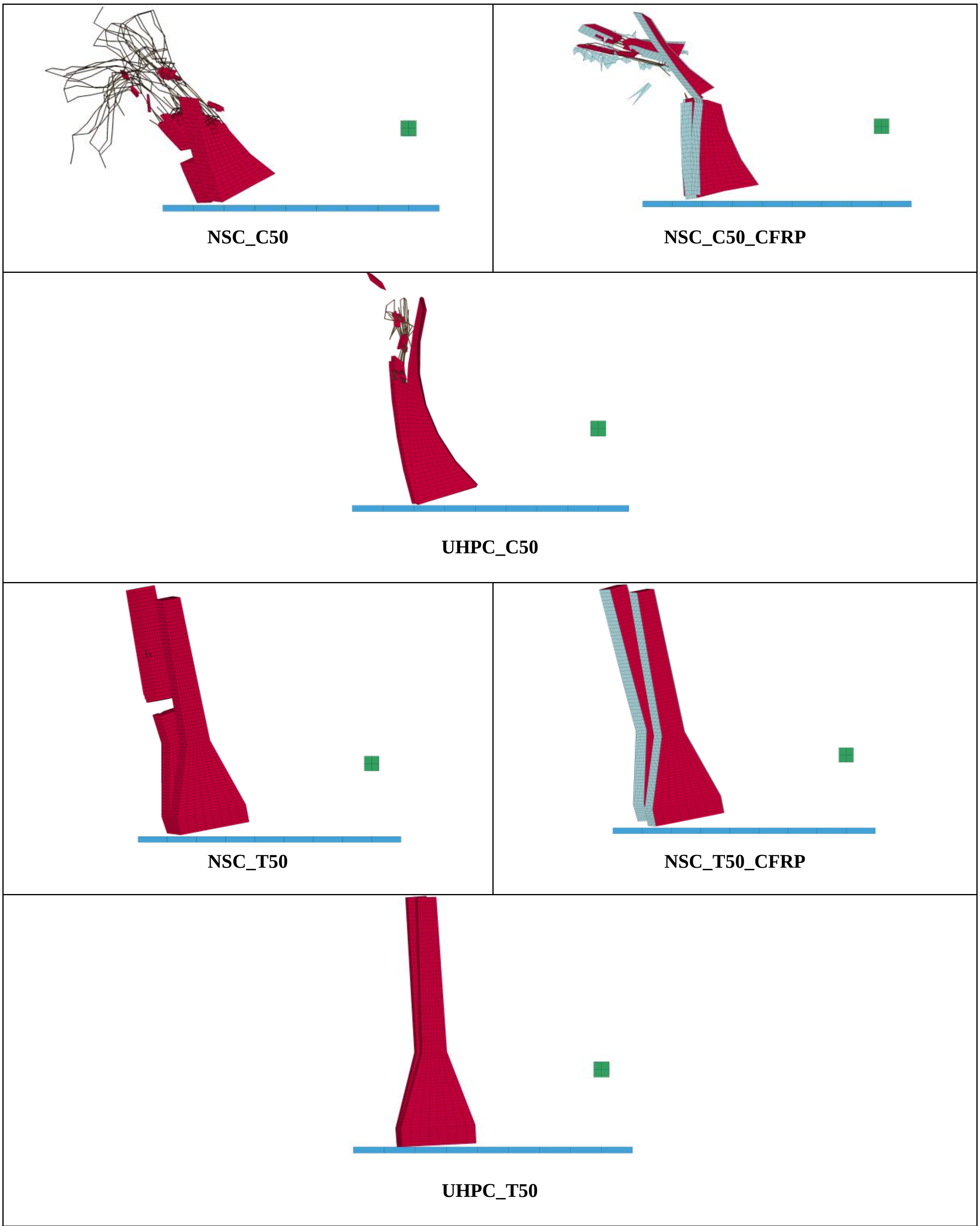

Figure 21: The damage of the fences due to 50 Kg at time 0.10 sec. (Side View**)**

Comparison of the results:

- In the case of using an explosive charge of 25Kg of TNT, the upper half of the (NSC_C25) fence has been collapsed and the explosion generates a lot of debris and fragments.
- Using CFRP with the (NSC_C25_CFRP) fence decreases the damage of the fence and decreases also the debris and fragments generation.

- The two middle units of the (NSC_T25) fence have a crack in the front side and not permeable to the backside, but no cracks are observed on the two outer units and the explosion generates little debris and fragments.
- In the case of using an explosive charge of 50kg of TNT, the (NSC_C50) fence has been totally collapsed and the explosion generates a lot of debris and fragments. The upper half of the (NSC_C50_CFRP) fence has been collapsed and the explosion generates debris and fragments lower than the (NSC_C50) fence.
- The upper half of the two middle units of the (UHPC_C50) fence has been collapsed, but no cracks are observed on the two outer units and the explosion generates high debris and fragments.
- The two middle units of the (NSC_T50) fence have divided into two parts and the rebars failure have occurred, but no cracks are observed on the two outer units and the explosion generates little debris and fragments.
- For the (UHPC_C25, NSC_T25_CFRP, UHPC_T25, NSC_T50_CFRP and UHPC_T50) fences, there are no cracks are observed on the fences and the explosion doesn`t generate any debris and fragments.
- It`s observed that externally bonded CFRP sheets may be effective in preventing or minimizing the damage level of the RC fences exposed to blast loads. The CFRP sheets show good potential for the strengthening of RC fences against blast loads and it is able to effectively contain the flying and scattered debris and fragments observed in unstrengthened fences. The CFRP sheets decrease the debris and fragments generation.

  Table 11 shows a comparison of the FE modelling results of the RC fences at time 0.10 sec.

Table 11: Comparison of the FE modelling results of the RC fences at time 0.10 sec.

Model ID	Debris and Fragments Generation	Damage Description	Model ID	Debris and Fragments Generation	Damage Description
NSC_C25	High	The upper half of the fence has been collapsed	**NSC_C50**	Very high	The fence has been collapsed.
NSC_C25_CFRP	Medium	The upper half of the fence has been collapsed	**NSC_C50_CFRP**	Medium	The upper half of the fence has been collapsed
UHPC_C25	No debris and fragments	No cracks are observed on the fence.	**UHPC_C50**	High	- The upper half of the two middle units of the fence has been collapsed. - No cracks are observed on the two outer units.
NSC_T25	Very low	A crack in the front side and not permeable to the backside.	**NSC_T50**	Medium	- The two middle units have divided into two parts and the rebars failure have occurred. - No cracks are observed on the two outer units.
NSC_T25_CFRP	No debris and fragments	No cracks are observed on the fence.	**NSC_T50_CFRP**	No debris and fragments	No cracks are observed on the fence.
UHPC_T25	No debris and fragments	No cracks are observed on the fence.	**UHPC_T50**	No debris and fragments	No cracks are observed on the fence.

VIII. Summary and Conclusions

This paper has presented a numerical study for evaluating the behaviour of the RC Curved and T-Shaped fences against blast loads and improving their blast resistance capacity**.** This analysis was carried out using the commercial program LS-DYNA which is a general-purpose finite element code for analysing the large deformation dynamic response of structures. The results were evaluated according to the damage and the value of the deformation. Validation has been performed by comparing FE modelling numerical results of a RC fence under blast detonations with available blasting experimental work in literature. RC fences with two different shapes (Curved and T-Shaped) using Normal Strength Concrete (NSC) have been examined against explosive charges. The influence of using Ultra-High-Performance Concrete (UHPC) and CFRP sheets for improving the blast resistance capacity has been investigated. From the study carried out through the present paper, the following points can be recorded:

1- The behaviour of the RC T-shaped fences against blast loads are much better than the behaviour of the RC Curved fences, because of the little damage and the low generation of the debris and fragments under the same quantity of blast with specified distance:

- The surface of the RC Curved fence collect and concentrate the blast wave in the curved shape and immediately cause big significant damage to the curved surface.
- The surface of Straight RC T-Shaped fence have no collect and concentrate the blast wave and therefore have less damage compared with the curved surface.

2- The usage of Ultra-High Performance Concrete or the externally bonded CFRP sheets significantly improves the blast resistance capacity of the RC fences. Little damage and the low generation of the debris and fragments compared with the original using of Normal Strength Concrete (NSC).

It`s recommended that further research with experimental tests be conducted for RC fences with different shapes, such as trapezoidal shape or convex shape. Additional research with experimental tests is needed for RC fences strengthened with CFRP against blast loads.

Acknowledgements

The authors would like to acknowledge the support of the Faculty of Engineering at Ain Shams University and The Egyptian Ministry of Interior. The authors would like to thank The General Department of Engineering Affairs, Egyptian Ministry of Interior for giving the opportunity to do this research and providing invaluable guidance throughout this research.

References

[1]. Muszynski LC, Purcell MR. Composite reinforcement to strengthen existing concrete structures against air blast. *J Compos Constr*. 2003;7(2):93-97. DOI:10.1061/(ASCE)1090-0268(2003)7:2(93)
[2]. Mutalib AA, Mussa MH, Hao H. Effect of CFRP strengthening properties with anchoring systems on P-I diagrams of RC panels under blast loads. *Constr Build Mater*. 2019;200:648-663. DOI:10.1016/j.conbuildmat.2018.12.169
[3]. Ghani Razaqpur A, Tolba A, Contestabile E. Blast loading response of reinforced concrete panels reinforced with externally bonded GFRP laminates. *Compos Part B Eng*. 2007;38(5-6):535-546. DOI:10.1016/j.compositesb.2006.06.016
[4]. Silva PF, Lu B. Improving the blast resistance capacity of RC slabs with innovative composite materials. *Compos Part B Eng*. 2007;38(5-6):523-534. DOI:10.1016/j.compositesb.2006.06.015
[5]. Schenker A, Anteby I, Gal E, et al. Full-scale field tests of concrete slabs subjected to blast loads. *Int J Impact Eng*. 2008;35(3):184-198. DOI:10.1016/j.ijimpeng.2006.12.008
[6]. Ha JH, Yi NH, Choi JK, Kim JHJ. Experimental study on hybrid CFRP-PU strengthening effect on RC panels under blast loading. *Compos Struct*. 2011;93(8):2070-2082. DOI:10.1016/j.compstruct.2011.02.014
[7]. Tai YS, Chu TL, Hu HT, Wu JY. Dynamic response of a reinforced concrete slab subjected to air blast load. *Theor Appl Fract Mech*. 2011;56(3):140-147. DOI:10.1016/j.tafmec.2011.11.002
[8]. Wang W, Zhang D, Lu F, Wang SC, Tang F. Experimental study on scaling the explosion resistance of a one-way square reinforced concrete slab under a close-in blast loading. *Int J Impact Eng*. 2012;49:158-164. DOI:10.1016/j.ijimpeng.2012.03.010
[9]. Wang W, Zhang D, Lu F, Wang S Chuan, Tang F. Experimental study and numerical simulation of the damage mode of a square reinforced concrete slab under close-in explosion. *Eng Fail Anal*. 2013;27:41-51. DOI:10.1016/j.engfailanal.2012.07.010
[10]. Pantelides CP, Garfield TT, Richins WD, Larson TK, Blakeley JE. Reinforced concrete and fiber reinforced concrete panels subjected to blast detonations and post-blast static tests. *Eng Struct*. 2014;76:24-33. DOI:10.1016/j.engstruct.2014.06.040
[11]. Foglar M, Hajek R, Kovar M, Štoller J. Blast performance of RC panels with waste steel fibers. *Constr Build Mater*. 2015;94:536-546. DOI:10.1016/j.conbuildmat.2015.07.082
[12]. Alsayed SH, Elsanadedy HM, Al-Zaheri ZM, Al-Salloum YA, Abbas H. Blast response of GFRP-strengthened infill masonry walls. *Constr Build Mater*. 2016;115:438-451. DOI:10.1016/j.conbuildmat.2016.04.053
[13]. G.Mahmoud et al. Protective Panels Design against Blast Loads. *Aust J Basic Appl Sci*. 2017;11(5)(April):143-156. doi:http://www.ajbasweb.com/old/ajbas/2017/April/143-156.pdf
[14]. Syed ZI, Raman SN, Ngo T, Mendis P, Pham T. The Failure Behaviour of Reinforced Concrete Panels Under Far-field and Near-field Blast Effects. *Structures*. 2018;14(2017):220-229. DOI:10.1016/j.istruc.2018.03.009
[15]. Adhikary S Das, Chandra LR, Christian A, Ong KCG. SHCC-strengthened RC panels under near-field explosions. *Constr Build Mater*. 2018;183:675-692. DOI:10.1016/j.conbuildmat.2018.06.199
[16]. Jin M, Hao Y, Hao H. Numerical study of fence type blast walls for blast load mitigation. *Int J Impact Eng*. 2019;131(November 2018):238-255. DOI:10.1016/j.ijimpeng.2019.05.007
[17]. Hao Y, Hao H, Shi Y, Wang Z, Zong R. Field Testing of Fence Type Blast Wall for Blast Load Mitigation. *Int J Struct Stab Dyn*. 2017;17(9):1-22. DOI:10.1142/S0219455417500997
[18]. Xiao W, Andrae M, Gebbeken N. Experimental and numerical investigations on the shock wave attenuation performance of blast walls with a canopy on top. *Int J Impact Eng*. 2019;131(March):123-139. DOI:10.1016/j.ijimpeng.2019.05.009
[19]. Xiao W, Andrae M, Ruediger L, Gebbeken N. Numerical prediction of blast wall effectiveness for structural protection against air blast. *Procedia Eng*. 2017;199:2519-2524. DOI:10.1016/j.proeng.2017.09.432
[20]. FEMA-428 /BIPS-07. Primer to Design Safe School Projects in Case of Terrorist Attacks and School Shootings. *FEMA-428/BIPS-07 Ed 2*. 2012;(January):317.
[21]. SPEC-905. *EGYPTIAN SPECIFICATION FOR BLAST RESISTANT BUILDINGS*. Cairo, Arab Republic Of Egypt: Ministry of Housing, Utilities & Urban Communities.; 2016. doi:https://www.scribd.com/document/436450770/EGYPTIAN-SPECIFICATION-FOR-BLAST-RESISTANT-BUILDINGS-SPEC-905
[22]. Karlos V, Solomon G. *Calculation of Blast Loads for Application to Structural Components*.; 2013. DOI:10.2788/61866
[23]. O.Hallquist J. LS-DYNA THEORY MANUAL. 2006.
[24]. Agardh L. Validation of Numerical simulations of structural response via material sample testing and field trials. 1999.
[25]. Leppänen J. Dynamic behaviour of concrete structures subjected to blast and fragment impacts. 2002.
[26]. Alia A, Souli M. High explosive simulation using multi-material formulations. *Appl Therm Eng*. 2006;26(10):1032-1042. DOI:10.1016/j.applthermaleng.2005.10.018

[27]. Zidan MK, Fayed MN, Elhosiny AM, Abdelgawad KM, Orfy HH. Modelling of damage patterns of RC concrete columns under demolition by blasting. *WIT Trans Built Environ*. 2014;141:95-111. DOI:10.2495/SUSI140091

[28]. Zukas, J. and Walters W. Explosive Effects and Applications. 1998.

[29]. Dobratz BM, Crawford PC. LLNL Explosives Handbook: Properties of Chemical Explosives and Explosive Simulants. 1985.

[30]. Maazoun A, Matthys S, Belkassem B, Lecompte D, Vantomme J. Blast response of retrofitted reinforced concrete hollow core slabs under a close distance explosion. *Eng Struct*. 2019;191(October 2018):447-459. DOI:10.1016/j.engstruct.2019.04.068

[31]. Vasudevan AK. FINITE ELEMENT ANALYSIS AND EXPERIMENTAL COMPARISON OF DOUBLY REINFORCED CONCRETE SLABS SUBJECTED TO BLAST LOADS. 2012.

[32]. O.Hallquist J. LS-DYNA Keyword Users Manual. 2010.

[33]. Thai DK, Kim SE. Numerical investigation of the damage of RC members subjected to blast loading. *Eng Fail Anal*. 2018;92(May):350-367. DOI:10.1016/j.engfailanal.2018.06.001

[34]. Thai D-K, Kim S-E. Prediction of UHPFRC panels thickness subjected to aircraft engine impact. *Case Stud Struct Eng*. 2016;5:38-53. DOI:10.1016/J.CSSE.2016.03.003

[35]. Chang FK, Chang KY. A Progressive Damage Model for Laminated Composites Containing Stress Concentrations. *J Compos Mater*. 1987;21(9):834-855. DOI:10.1177/002199838702100904

[36]. Elsanadedy HM, Almusallam TH, Alsayed SH, Al-Salloum YA. Flexural strengthening of RC beams using textile reinforced mortar - Experimental and numerical study. *Compos Struct*. 2013;97:40-55. DOI:10.1016/j.compstruct.2012.09.053

[37]. Elsanadedy HM, Almusallam TH, Alsayed SH, AL-Salloum YA. Experimental and FE study on RC one-way slabs upgraded with FRP composites. *KSCE J Civ Eng*. 2015;19(4):1024-1040. DOI:10.1007/s12205-013-0689-y

[38]. Almusallam TH, Elsanadedy HM, Al-Salloum YA. Effect of longitudinal steel ratio on behavior of RC beams strengthened with FRP composites: Experimental and FE study. *J Compos Constr*. 2015;19(1):1-18. DOI:10.1061/(ASCE)CC.1943-5614.0000486

[39]. Almusallam T, Al-Salloum Y, Elsanadedy H, Alshenawy A, Iqbal R. Behavior of FRP-Strengthened RC Beams with Large Rectangular Web Openings in Flexure Zones: Experimental and Numerical Study. *Int J Concr Struct Mater*. 2018;12(1). DOI:10.1186/s40069-018-0272-5

[40]. Lu XZ, Teng JG, Ye LP, Jiang JJ. Bond-slip models for FRP sheets/plates bonded to concrete. *Eng Struct*. 2005;27(6):920-937. DOI:10.1016/j.engstruct.2005.01.014

[41]. Lu XZ, Teng JG, Ye LP, Jiang JJ. Intermediate crack debonding in FRP-strengthened RC beams: FE analysis and strength model. *J Compos Constr*. 2007;11(2):161-174. DOI:10.1061/(ASCE)1090-0268(2007)11:2(161)

[42]. Dolce F. Blast Impact Simulation on Composite Military Armours. 2009:121. https://researchportal.bath.ac.uk/en/publications/blast-impact-simulation-on-composite-military-armours.

Mohamed A. Basset, et. al. “Evaluating and improving the blast resistance capacity of the RC fences.” *IOSR Journal of Mechanical and Civil Engineering (IOSR-JMCE)*, 17(3), 2020, pp. 26-47.